The 2009 IEEE/RSJ International Conference on
Intelligent Robots and Systems
October 11-15, 2009 St. Louis, USA

Proposal and Development of Arrayed Sole Sensor for Legged Robot and Contact Force Detection Using Neural Networks

Seiji Aoyagi, *Member, IEEE,* Takashi Matsuda, Yuuki Ikejiri, Masato Suzuki, Kenji Inoue

***Abstract*—Recently multi-legged walking robots are widely developed. For these robots to walk safely, a sole sensor with high performance is desired. In the present paper, an arrayed type tactile sensor made of flexible silicone rubber, which is based on micro-electro-mechanical-systems (MEMS) technology, was developed. This sensor was applied as a sole sensor of a legged mobile robot. By processing the force data from many sensing elements using neural networks, information of contact force, i.e., three dimensional *x*, *y*, and *z* components of force vector, was able to be detected, which was confirmed by both simulation and experiment.**

I. Introduction

RECENTLY, the multi-legged walking robots are widely developed. Since this type robot has high ability of traversing cluttered environment with a rugged surface, the application of it to a complicated situation such as a disaster site is expected. In the situation that the ground surface severely ungulates, or visual sensors cannot be used owing to the darkness, a sole sensor to detect the contact force is desired for performing the stable walking.

Inoue, one of the authors of the present paper, has developed a mobile robot with six legs, which can switch the function of each link mechanism between arm and leg for adapting the environmental situation [1]. Aoyagi, one of the authors of the present paper, is developing an arrayed tactile sensor using micro-electro-mechanical-systems (MEMS) technology. The structural material of it is polydimethylsiloxane (PDMS), which is a kind of silicone rubber [2], so the sensor is flexible to fit the surface of robot finger, robot sole, etc. The sensor is composed of arrayed sensing elements, each of which detects its capacitance change with respect to the displacement of the sensing surface in *z* (vertical) direction. In the present paper, this sensor is applied to a sole sensor of the abovementioned legged mobile robot. By processing the force data from many sensing elements by neural networks (NN), information of contact force, i.e., three dimensional *x*, *y*, and *z* components of force vector, can be detected [3].

Manuscript received March 4, 2009. This is a product of research which was financially supported by the Kansai University Research Grants: Grant-in-Aid for Joint Research, 2008. "Application of MEMS Arrayed Tactile Sensor to Sole of Multi-Legged Robot".

S. Aoyagi, T. Matsuda, Y.Ikejiri, and M. Suzuki are with Department Mechanical Engineering, Kansai University, Suita, OSAKA 564-8680, JAPAN (Corresponding author: Seiji Aoyagi, phone: +81-6-6368-0823; fax:+81-6-6330-3154; e-mail: aoyagi@iecs.kansai-u.ac.jp).

K. Inoue is with Department Bio-System Engineering, Yamagata University, YAMAGATA, JAPAN (e-mail: inoue@yz.yamagata-u.ac.jp).

The human skin contains numerous force-sensing receptors distributed horizontally and vertically at intervals of about 1 mm [4]. It is technically difficult to fabricate a sensor having numerous force sensing elements. Attempts have been made to solve this problem by analyzing stress distribution optically [5]. Ascari et al. once transform the force data of massive tactile sensing elements to a tactile image, followed by image signal processing, which is effective to detect contact position and slippage for successful *pick and lift* tasks [6].

MEMS technology is effective for fabricating a tactile sensor of directly processing force data, i.e., not processing optically transformed data, since numerous arrayed miniature force sensors with uniform performance are fabricated on a silicon wafer with fine resolution of several microns. Tactile sensors proposed and developed based on MEMS are classified to piezoresistive [7] and capacitive [8]. We focus on capacitive tactile sensors, mainly considering fabrication ease that lowers cost.

Human tactile sensing receptors detect force magnitude but not its direction. The brain synthesizes nerve signals from receptors and obtains cutaneous stress distribution to finally recognize the direction. If individual receptors (sensors) could detect the 3-D force direction, however, signal processing in tactile sensing would become easier and more accurate. Even though, we use an array of single axis sensors at present, and using a 3-D sensor is future work.

Several tactile sole sensors are reported for the use of stable walking of humanoid robots [9-11], in which the stress distribution inside the sole is discussed. Compared with these reports, a method of acquiring the contact force is proposed in the present paper, in which the outputs of many sensing elements, i.e., stress distribution, are processed by NN. Note that similar challenges are proposed and conducted as cellular nonlinear/neural networks (CNN) [6].

The composition of this paper is organized as follows: first, the validity of measuring principle using arrayed sensor and NN was confirmed by the simulation, in which the stress distribution of the PDMS sensor sheet was given by finite element method (FEM) analysis. The optimal number and the size of sensing elements of the array were also investigated by this simulation. Second, an arrayed sensor was practically fabricated. Finally, the performance of the sensor was investigated by an experiment, in which various forces were applied by changing its magnitude and direction, and they were detected by both the developed arrayed sensor and a commercial multi-axes force sensor for reference.

The features of this research are as follows: 1) The space required for installing the entire measuring system becomes smaller compared to the case that a commercial multi-axes force sensor is installed at the robot's ankle part. 2) Since the sensor can be set near the contact surface compared with the case that a multi-axes force sensor is set to the ankle part, higher accuracy of force measurement is expected. 3) The sensor is expected to be economical compared with multi-axes force sensors, since MEMS sensor has a merit of fabricating numerous small sensors with small cost due to its batch process using a photolithography technique.

II. Arrangement of Sensor and Legged Robot

The robot to which the sole sensor is attached has six legs, as shown in Fig. 1. Each leg can be used as an arm depending on the environmental situation, so the size of the robot is miniaturized compared with a normal robot equipped with arm mechanism and leg (or wheel) mechanism separately. Moreover, the traverse ability and flexibility on different environmental situation are expected to be excellent. The small and light sensor fabricated by MEMS technique is suitable for the sole sensor of this robot, since it does not degrades the robot's advantage of being small and light.

The overview of the leg of the robot is shown in Fig. 2(a). The length of each leg, which has three joints, is 350 mm at full expansion. There is a hemispheric hollow of 20 mm diameter in the tip part of each leg, as shown in Fig. 2(b). A rubber ball is set in the hollow, as shown in Fig. 2(c).

An arrayed tactile sensor is set between two rubber hemispheres, which are made by cutting a rubber ball into two halves. They are fixed again to one spherical ball, and attached to the hollow at the leg's tip using adhesive resin.

III. Simulation Analysis of Optimal Number and Size of Sensing Elements of Arrayed Sensor

A. Simulation Model

The force is assumed to be applied from the floor to the ball. The force is applied by changing its direction at every 10 deg within the range that θ_1 is from 0 to 90 deg, and θ_2 is from 40 to 90 deg, i.e., within the 1/4 space, as shown in Fig. 3.

Here, if the external load force besides from the floor exists or if the rubber ball is largely deformed, the applied total force does not exactly go through the center of the sensor. The investigation on this effect should be the projected work.

As FEM software, ANSYS® is used. The meshed model used for simulation is shown in Fig. 4(a), in which two hemispheres are assumed to be the halves divided from the rubber ball, a thin block put between the two hemispheres is assumed to be the PDMS sensor sheet, and the block on the surface of the upper hemisphere is assumed to be the floor. Namely, the floor, the sensor, and the ball are turned upside down in this FEM model, considering the limit of memory resource of computer. The materials are set as follows: rubber ball is made of butadiene rubber (Young's modulus E is 5.2 MPa, Poisson ratio ν is 0.49, density ρ is 910 kg/m^3), the sensor sheet is made of PDMS (E is 3.0 MPa, ν is 0.40, ρ is 1500 kg/m^3), and the floor is made of cement (E is 25 GPa, ν is 0.15, ρ is 2500 kg/m^3). An example of the result, in which the distribution of stress in vertical (z) direction is analyzed, is shown in Fig. 4(b).

B. Analysis (Preparation of Training data and verification data for NN)

The stress distribution in the sensor sheet is obtained by

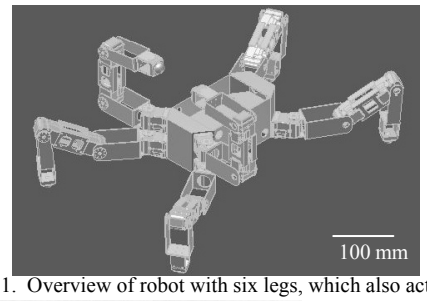

Fig. 1. Overview of robot with six legs, which also act as arms.

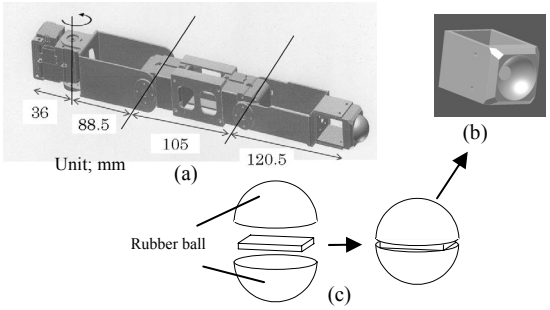

Fig. 2. Robot's leg and sole sensor, (a) robot leg, (b) tip of leg with a hollow, and (c) attachment of sensor to a rubber ball.

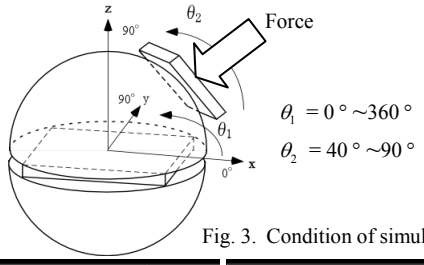

Fig. 3. Condition of simulation.

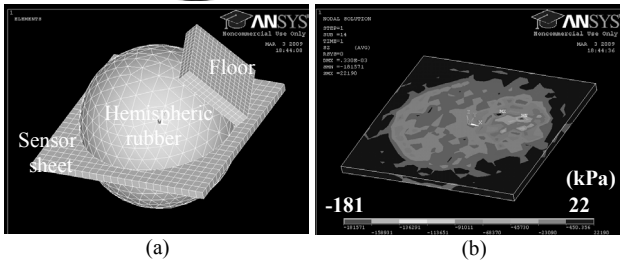

Fig. 4. FEM simulation, (a) model, and (b) example of stress distribution in case that θ_1 =20 ° , θ_2 =40 ° (See Fig. 3).

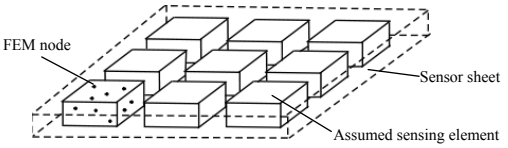

Fig. 5. The data of stress in z direction of FEM nodes within the assumed rectangular space are averaged, and the averaged value is assigned to the sensing element as its output.

FEM analysis. Considering the symmetry, the data in the whole space is obtained, which are totally 181 combinations of θ_1 and θ_2. They compose the training data set for the NN. As the verification data set for confirming the generalization ability of the NN, the stress distributions at 180 combinations of θ_1 and θ_2 are used, which are shifted from those of training data set by 5 deg in θ_1 and θ_2, respectively.

The rectangular divided spaces are assumed in the sensor sheet, which are correspondent to the sensing elements of the arrayed sensor, as shown in Fig. 5. The stress distribution obtained by FEM simulation is the cluster of stress datum at each node of meshed model. The data of stress in z direction of FEM nodes within the abovementioned assumed rectangular space are averaged, and the averaged value is assigned to the sensing element as its output.

After assigning the FEM result to each sensing element, every data are normalized so as that the maximum stress value is to be 1, and input to the NN.

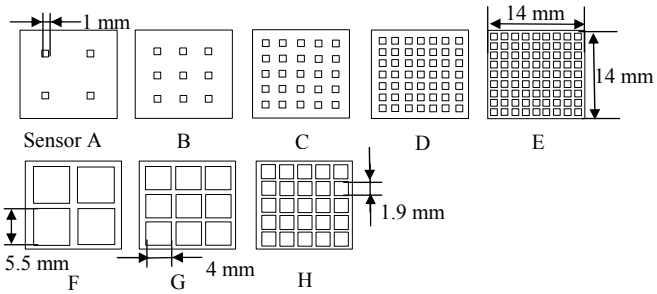

Fig. 6. Assumed sensors having different number of sensing elements and different sensing area of each element.

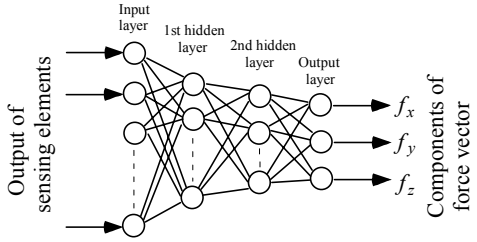

Fig. 7. Composition of neural networks.

TABLE I
THE NUMBER OF NEURONS OF EACH LAYER

	Input	1st hidden	2nd hidden	Output
A, F	4	120	60	
B, G	9	180	90	3
C, H	25	500	250	(f_x, f_y, f_z)
D	49	490	245	
H	81	810	405	

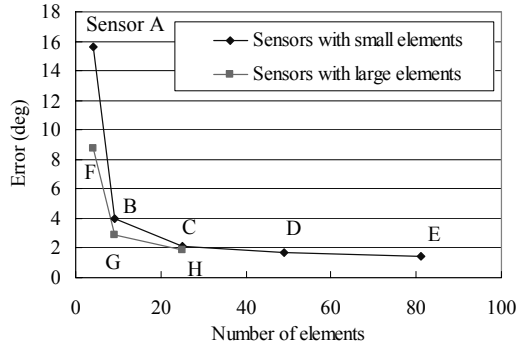

Fig. 8. Errors of force direction for verification data set.

C. Assumed sensors having different number of sensing elements and different sensing area of each element

Several types of sensor, of which total size is fixed to 14 mm square, are assumed by changing the number of sensing elements and changing the area of sensing surface of each element, as shown in Fig. 6.

While the area of each element in Sensor A, B, C, D and E is fixed to 1 mm square, the number of elements of them is varied at 4, 9, 25, 49, and 81, respectively.

While the number of elements of Sensor F coincides with that of Sensor A, the area of each element of Sensor F is larger than that of Sensor A. So do Sensor G and Sensor B, Sensor H and Sensor C.

D. Neural Networks

The FEM simulated outputs of all the sensing elements are input to the NN, which outputs three components f_x, f_y and f_z of force vector $\boldsymbol{f} \in R^3$. The composition of NN is shown in Fig. 7. The number of neurons of each layer of the NN is shown in Table I. The employment of two hidden layers, and the definition of the number of neurons of them are based on the adjustment by trial and error.

The connection weights between adjacent neurons in the NN are obtained by supervised learning. As a learning method that decreases the error between NN outputs and training data, RPROP method [12] modifying the well-known back propagation (BP) method is adopted, which speeds up the convergence calculation by several tens times compared with the BP method. After supervised learning, verification data are input to the NN for confirming the effectiveness of the NN.

E. Results of Simulation

The error between the components of applied force vector $\boldsymbol{f}_{\text{in}}$ and those of output force vector of the NN $\boldsymbol{f}_{\text{out}}$ was estimated by the angle between $\boldsymbol{f}_{\text{in}}$ and $\boldsymbol{f}_{\text{out}}$. The average of errors for 180 verification data set for Sensor A~F are shown in Fig. 8. Adding to say, almost the same results were obtained by the simulation, in which the 5% random error is added to each output of the sensing elements (data were omitted).

Looking at this figure, the error of force direction becomes smaller as the number of sensing elements increases. This trend, however, is saturated if the number is beyond around 10. Also, the error becomes smaller as the area of each sensing element increases. Although this trend is conspicuous in the case that the number of sensing elements is 4, i.e., in the comparison between Sensor A and Sensor F, it is not so conspicuous in the comparison between Sensor B and Sensor G, and that between Sensor C and Sensor H.

Considering both the abovementioned results and the factor that the large number of sensing elements requires large cost of fabrication/assembling, the number of sensing elements is set to 9 (=3×3). And the area of sensing element is fixed to 4 mm square. Namely, Sensor G is adopted in the

following part of this paper.

F. Simulation of Practical Sensor Composed of 3×3 Capacitive Sensing Elements

Taking account of the practical sensor structure, the detailed simulation model is employed, as shown in Fig. 9(a). An example of the result, in which the distribution of displacement in vertical (z) direction was analyzed, is shown in Fig. 9(b). By applying the multiphysics mode of ANSYS software to this model, the capacitance changes ΔC of sensing elements caused by the stress distribution are simulated. Then, the data of ΔC are input to NN, the composition of which is shown in Fig. 10.

The training data set is prepared by changing the force direction of θ_1 and θ_2, and changing the force magnitude $|\boldsymbol{f}|$

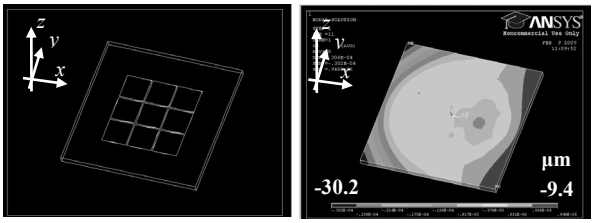

(a) (b)

Fig. 9. Detailed FEM simulation, (a) model with 9 sensing elements, and (b) example of distribution of displacement in z direction in case that θ_1=20 ° , θ_2 =40 ° .

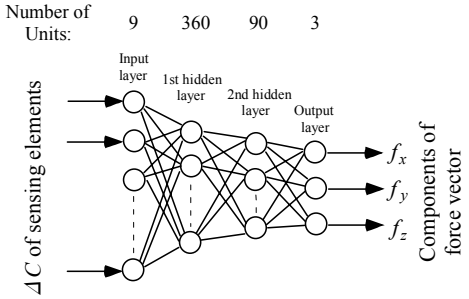

Fig. 10. Composition of neural networks for detailed sensor

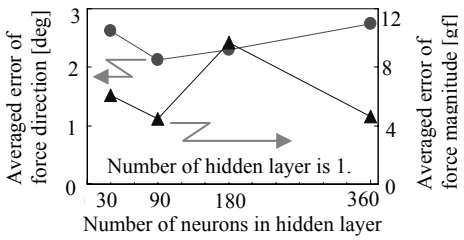

Fig. 11. Effect of neuron number on performance (simulation).

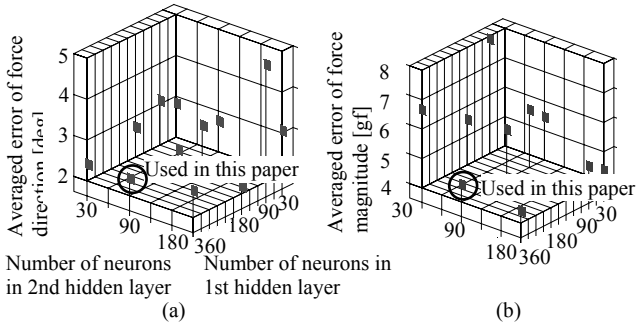

(a) (b)

Fig. 12. Effect of neuron number of 1st and 2nd hidden layers on performance (simulation), (a) error of force direction, and (b) error of force magnitude.

at 50 gf and 150 gf. The number of combinations of θ_1, θ_2, and $|\boldsymbol{f}|$ for training is 362 in total. The verification data set is prepared by shifting the stress angles of θ_1 and θ_2 by 5 deg, respectively, while $|\boldsymbol{f}|$ is fixed to 100 gf. The number of combinations of θ_1, θ_2, and $|\boldsymbol{f}|$ for verification is 180 in total.

After supervised learning of NN, the simulation was carried out for verification data set. The resultant averaged error of force direction was 2.4 deg. This value is 0.7% of the full range of 360 deg. The averaged error of force magnitude was 5.3 gf. This value is 5.3% of applied force of 100 gf. Namely, it is confirmed that this sensor has possibility of sensing the force direction and its magnitude within several percent of applied values, of which order is comparable with that of a commercial multi-axes force sensor [13].

G. Effect of Number of Hidden Layers and Neurons

The effect of number of hidden layers and neurons on the NN performance is investigated in the simulation. The results are shown in Figs. 11 and 12. The performance of employing two hidden layers is better than that of employing one hidden layer, even the extent is a little. Not to mention that too small number of neurons, too large number of neurons is also not effective for increasing the performance.

IV. Fabrication of Practical Sensor

Taking account of simulation results, a practical sensor

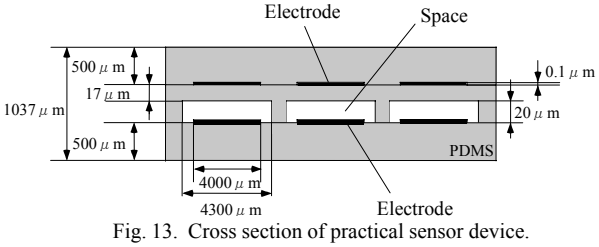

Fig. 13. Cross section of practical sensor device.

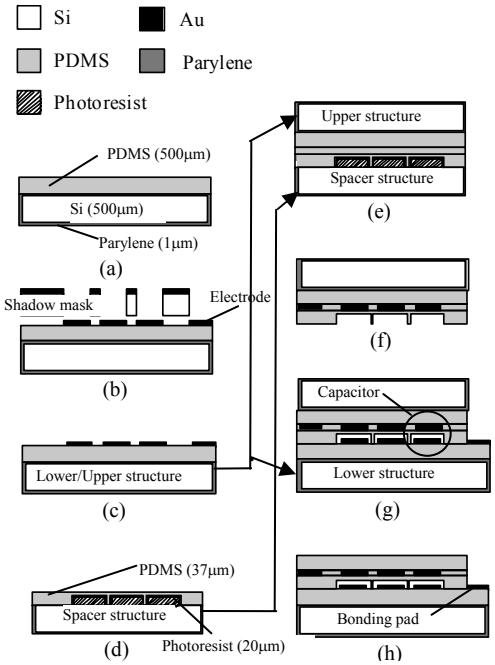

Fig. 14. Process flow of arrayed tactile sensor.

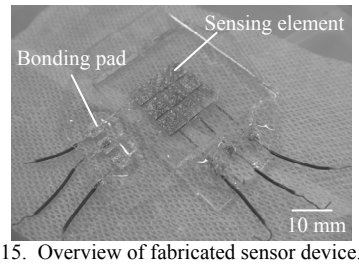

Fig. 15. Overview of fabricated sensor device.

device is designed, of which cross section including size is shown in Fig. 13.

The fabrication process is as follows: Parylene (1 μm) for anti-stiction layer is conformally deposited on a silicon wafer, the only function of which is to support the PDMS layer. Then, PDMS (500 μm) is spin-coated at 400 rpm, 20 sec (Fig. 14(a)). Au (0.1 μm) is deposited for electrodes using the shadow mask method (Fig. 14(b)). At this step, the lower structure is completed (Fig. 14(c)). The upper structure is also fabricated by the same process.

Next, the spacer structure, which bears a number of concave space serving as the gap between two electrodes of a capacitor, is fabricated. For this purpose, Parylene (1 μm) is deposited on patterned photoresist (20 μm), then, PDMS (37 μm) is spun on it (Fig. 14(d)).

The upper structure and the spacer structure are bonded with each other by applying heat using a hot plate of 100 C° (Fig. 14(e)).

The bonded structure is peeled off from the silicon wafer. Concave spaces are formed as negative of the patterned photoresist (Fig. 14(f)). The lower structure is bonded with the spacer structure by applying heat. Each sealed concave space has lower and upper electrodes, forming a capacitor (Fig. 14(g)). The upper silicon wafer is taken away from the upper structure (Fig. 14(h)).

The photograph of overview of fabricated sensor is shown in Fig.15. Gold electrodes for 9 (=3×3) capacitive sensing elements are seen on a transparent PDMS sheet. Also, the bonding pads are seen, each of which is connected to three sensing elements on a row or a column. By selecting a pad for a row and that for a column, one sensing element on the intersection of the row and the column can be designated.

V. Experiment for Performance Estimation of Fabricated Sole Sensor

A. Experimental Setup

The schematic and photographic overviews of the experimental setup are shown in Figs. 16(a) and (b), respectively. The fabricated sensor is placed between the two hemispheric rubber balls, and the assembled ball is set in the hollow at the tip of the robot's leg. The bottom surface of a stick is assumed to be the contact area of the floor.

While the stick is kept to push against the rubber, it is fixed between the two horizontal rail parts tightly by screws. The directions of θ_1 and θ_2 are arbitrary defined by adjusting the horizontal and vertical angles of the stick. At the bottom of the experimental setup, a commercial multi-axes force sensor (BL Autotech Corp., Type MINI 4/20) is incorporated for the reference, of which specification is shown in Table II.

B. Confirmation of Capacitance Change (Comparison with Simulation Data)

The stick was pushed against the sensor, then, the capacitance change of each sensing element was measured one by one by using a LCR meter (Agilent Corp., Type E4980A, resolution is 1fF). Knowing the applied force by the multi-axes force sensor, the multiphysic FEM simulation was carried out according to the procedure mentioned in Section III F, finally the capacitance changes of all the sensing elements are simulated.

The results of comparison with measured and simulated capacitance changes of 9 elements are shown in Figs. 17(a) and (b), which are the case that (θ_1, θ_2)= (0°, 45°) . Looking at this figure, experimental distribution of capacitance changes resembles simulation distribution.

The error may be mainly caused by the fabrication error of the sensor device, e.g., the gap length between the electrodes of the capacitive sensing element could not be achieved as the designed value. The further investigation of the cause of the error and the improvement for decreasing the error are left in the future work.

C. Detection of Components of Applied Force Vector (Comparison with Multi-Axes Force Sensor)

The same procedure was carried out as mentioned in Section III F using the experimental data of capacitance changes. Training data set of 362 pairs of capacitance

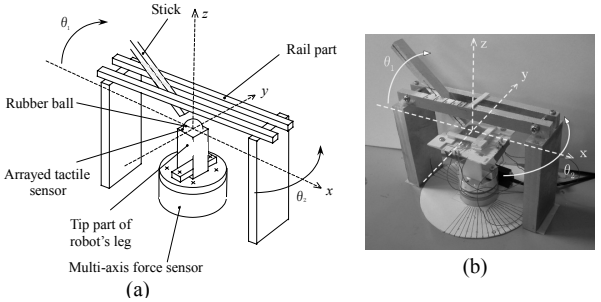

Fig. 16. Overview of experimental setup, (a) schematic, (b) photograph.

TABLE II
Performance of Commercial Multi-axis Force Sensor

Rated value [*fx, fy, fz* (kgf)]	4, 4, 8
Resolution [*fx, fy, fz* (gf)]	4, 4, 12
Linearity	1.5% of rated value

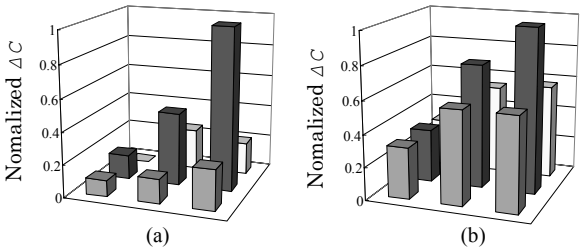

Fig. 17. Distribution of capacitance changes of sensing elements in the case of $\theta_1 = 0°$ and $\theta_2 = 45°$, (a) detected by the developed sensor, (b) simulation results.

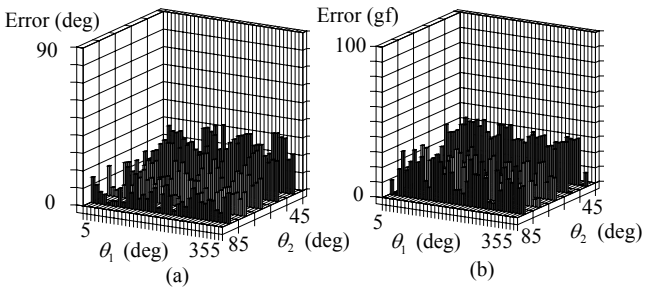

Fig. 18. Error distribution, (a) direction, and (b) magnitude (applied 100gf).

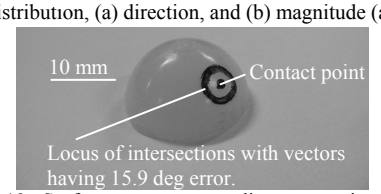

Fig. 19. Surface area corresponding to experimental force directional error of 15.9 deg.

changes, in which θ_1, θ_2, and $|\boldsymbol{f}|$ are variously changed, was prepared from the experimental data obtained by the fabricated practical sensor. Verification data set of 180 pairs of capacitance changes was also prepared from the experimental data in the same way. After the supervised learning of NN, the verification data set is applied to the NN, then the NN outputs are compared with the direction and the magnitude of the applied force.

The experimental results are shown in Figs. 18(a) and (b), which exhibit the error of force direction and the error of force magnitude, respectively. Looking at these figures, the resultant averaged error of force direction is 15.9 deg, and that of force magnitude is 18.7 gf. These errors are larger than those obtained by the simulation (see Section III F. They were 2.4 deg and 5.3 gf, respectively). The errors are supposedly caused by the fabrication error, as mentioned in the previous paragraph. These errors should be decreased in the projected work by improving the fabrication precision.

In the end, although the problem of non-negligible errors exists, it is confirmed that the proposed sensor can detect roughly the direction and the magnitude of the contact force. For simple comprehension, the surface area corresponding to the experimental error of 15.9 deg is shown in Fig. 19. In this figure, the black point shows the contact point at which the force is applied, and the black circumference shows the locus of intersections between the force vectors with 15.9 deg error and the surface of the ball.

VI. Conclusion

An arrayed type tactile sensor made of flexible silicone rubber, which is based on MEMS technology, was developed. This sensor was applied as a sole sensor of a legged mobile robot. By processing the force data from many sensing elements by neural networks (NN), information of contact force, i.e., three dimensional x, y, and z components of force vector, is expected to detect.

The sensor was practically fabricated and its performance was investigated by both FEM simulation and experiment, in which various forces are applied by changing its magnitude and direction. The averaged error in simulation was 2.4 deg and 5.3 gf, which are several percent of maximal applied values. Although they were degraded to 15.9 deg and 18.7 gf in the experiment, the validity of the measuring principle and the basic potential for the application of the sole sensor of a legged robot were confirmed.

To reduce the practical errors, an approach to increase the sensitivity using a gelled polyurethane thin film is on going. Its Young's modulus is 20 kPa, which is less than 1/100 compared with PDMS, and no gaps are provided between upper/lower electrodes for preventing stiction problems [14].

Acknowledgment

This is a product of research which was financially supported by the Kansai University Research Grants: Grant-in-Aid for Joint Research, 2008. "Application of MEMS Arrayed Tactile Sensor to Sole of Multi-Legged Robot".

References

[1] K. Inoue and K. Ooe, "Six-Legged Robots Capable of Locomotion and Manipulation in Three Modes," in *Proc. JSME Conf. Robotics and Mechatronics*, Nagano, Japan, 2008, 1A1-E04.

[2] D. Ono, T. Fukutani, and S. Aoyagi, "Development of an Arrayed Tactile Sensor Having Four Stories and Recognition of Contact State Using Neural Networks," *IEEJ Trans. SM*, vol. 128, no.5, pp.246-251, 2008.

[3] T. Tanaka and S. Aoyagi, "Recognition of Contact State of Four Layers Arrayed Type Tactile Sensor by Supervised Learning," in *Proc. JSME Conf. Robotics and Mechatronics*, Waseda, Japan, 2006, 2A1-E29.

[4] T. Maeno, Structure and Function of Finger Pad and Tactile Receptors," *J. The Robotics Society of Japan*, vol. 18, no. 6, pp. 767-771, 2000.

[5] K. Kamiyama, H. Kajimoto, M. Inami, N. Kawakami, and S. Tachi, "Development of a Vision-based Tactile Sensor," *Trans. Institute of Electrical Engineers of Japan*, vol.123, no.1, pp. 16-22, 2003.

[6] L. Ascari, U. Bertocchi, P. Corradi, C. Laschi, and P. Dario, "Bio-inspired Grasp Control in a Robotic Hand with Massive Sensorial Input", *Biological Cybernetics*, vol. 100, no.2, pp. 109-128, 2009.

[7] H. Takao, K. Sawada, and M. Ishida, "Multifunctional Smart Tactile-Image Sensor with Integrated Arrays of Strain and Temperature Sensors on Single Air-Pressurized Silicon Diaphragm," in *Proc. IEEE Transducers '05*, Seoul, Korea, 2005, pp. 45-48.

[8] B. J. Kane, M. R. Cutkosky, and G. A. Kovacs, "A Tactile Stress Sensor Array for Use in High-Resolution Robotic Tactile Imaging," *J. Microelectromechanical Systems*, vol.9, no.4, pp. 425-434, 2000.

[9] Y. Tanida, K. Abe, A. Konno, and M. Uchiyama, "Design and Development of a H-slit Type Ground Reaction Force Sensor for a Humanoid Robot," in *Proc. JSME Conf. Robotics and Mechatronics*, Nagoya, Japan, 2004, 2A1-H-74.

[10] G. Kinoshita, T. Kimura, and M. Shimojo, "Dynamic Sensing Experiments of Reaction Force Distributions on the Sole of a Walking Humanoid Robot," *in Proc. Intelligent Robots and Systems, 2003. (IROS 2003)*. Proceedings. 2003 IEEE/RSJ International Conference on Volume 2, 27-31 Oct. 2003 Page(s):1413 - 1418 vol.2.

[11] A. Sekiguchi, T. Suzuki, Y. Atobe, Y. Tsumaki, and D. N. Nenchev, "On the Role of the Foot Shape of a Humanoid Robot," in *Proc. JSME Conf. Robotics and Mechatronics*, Kobe, Japan, 2005, 1P2-S-043.

[12] M. Riedmiller and H. Braun, "A Direct Adaptive Method for Faster Backpropagation Learning: The RPROP Algorithm," in *Proc. IEEE Intl. Conf. Neural Networks*, San Francisco, CA, USA, 1993.

[13] BL AUTOTEC.LTD, Performance of Force Sensor (MINI 4/20) "https://www.bl-autotec.co.jp/FA/01force/01_03_mini.html"

[14] M. Suzuki, Y. Ikejiri, T. Fukutani, and S. Aoyagi, "Tactile Sensor Using Gelled Poly-Urethane Ultrathin Film," to be presented in *IEEE Sensors 2009 Conf.*, 27 Oct. 2009, Christchurch, New Zealand.